

Surgical Aggregation: A Federated Learning Framework for Harmonizing Distributed Datasets with Diverse Tasks

Pranav Kulkarni¹

PKULKARNI@SOM.UMARYLAND.EDU

Adway Kanhere^{1,2}

AKANHERE@SOM.UMARYLAND.EDU

Paul H. Yi¹

PYI@SOM.UMARYLAND.EDU

Vishwa S. Parekh¹

VPAREKH@SOM.UMARYLAND.EDU

¹ University of Maryland Medical Intelligent Imaging (UM2ii) Center

University of Maryland School of Medicine

Baltimore, MD 21201

² Department of Biomedical Engineering, Johns Hopkins University, Baltimore, MD 21218

Editors: Under Review for MIDL 2023

Abstract

AI-assisted characterization of chest x-rays (CXR) has the potential to provide substantial benefits across many clinical applications. Many large-scale public CXR datasets have been curated for detection of abnormalities using deep learning. However, each of these datasets focus on detecting a subset of disease labels that could be present in a CXR, thus limiting their clinical utility. Furthermore, the distributed nature of these datasets, along with data sharing regulations, make it difficult to share and create a complete representation of disease labels. We propose surgical aggregation, a federated learning framework for aggregating knowledge from distributed datasets with different disease labels into a ‘global’ deep learning model. We randomly divided the NIH Chest X-Ray 14 dataset into training (70%), validation (10%), and test (20%) splits with no patient overlap and conducted two experiments. In the first experiment, we pruned the disease labels to create two ‘toy’ datasets containing 11 and 8 labels respectively with 4 overlapping labels. For the second experiment, we pruned the disease labels to create two disjoint ‘toy’ datasets with 7 labels each. We observed that the surgically aggregated ‘global’ model resulted in excellent performance across both experiments when compared to a ‘baseline’ model trained on complete disease labels. The overlapping and disjoint experiments had an AUROC of 0.87 and 0.86 respectively, compared to the baseline AUROC of 0.87. We used surgical aggregation to harmonize the NIH Chest X-Ray 14 and CheXpert datasets into a ‘global’ model with an AUROC of 0.85 and 0.83 respectively. Our results show that surgical aggregation could be used to develop clinically useful deep learning models by aggregating knowledge from distributed datasets with diverse tasks, a step forward towards bridging the gap from bench to bedside.

Keywords: Deep learning, federated learning, surgical aggregation, chest x-ray, classification.

1. Introduction

Chest X-Ray (CXR) is the most commonly ordered medical imaging study globally and is critical for screening many life threatening conditions like pneumonia. As a result, many large-scale public CXR datasets have been released through curation of Wang et al. (2017), Irvin et al. (2019), Johnson et al. (2019), and Nguyen et al. (2022) for the purpose of

training clinically-useful deep learning models for detection of diseases in the thorax. These, in turn, have resulted in numerous narrowly-focused ‘toy’ datasets as part of data science competitions hosted on platforms like Kaggle, like the RSNA pneumonia detection challenge (Shih et al., 2019), resulting in expert-level performance for single disease diagnoses.

The release of both large-scale datasets as well as toy datasets has spearheaded the utility of deep learning in medical imaging by providing expert-level detection of diseases using CXRs. Unfortunately, due to the nature of curating large-scale datasets, these datasets are often distributed and focus on detecting different disease labels. As a result, these datasets can be considered ‘incomplete’ since information about labels present in one dataset may not be available in another dataset. For example, the NIH Chest X-Ray 14 (‘NIH’) (Wang et al., 2017) dataset consists of 14 labels while the CheXpert and MIMIC-CXR datasets (Irvin et al. (2019), Johnson et al. (2019) consist of 13 labels (excluding the label for normal). Despite having 7 labels in common, as shown in Figure 1, all three datasets are distributed and incomplete. As a result, naïvely training a deep learning model on all three datasets, without harmonizing them first, could lead to incomplete and inaccurate representation of the distribution.

NIH	MIMIC-CXR/CheXpert
Atelectasis	Atelectasis
Cardiomegaly	Cardiomegaly
Consolidation	Consolidation
Edema	Edema
Effusion	Effusion
Emphysema	Enlarged Cardiom.
Fibrosis	Fracture
Hernia	Lung Lesion
Infiltration	Lung Opacity
Mass	Pleural Other
Nodule	Pneumonia
Pleural_Thickening	Pneumothorax
Pneumonia	Support Devices
Pneumothorax	-

Figure 1: Comparison of disease and finding labels between NIH and CheXpert datasets. Overlapping labels highlighted in blue.

Similarly, while toy datasets are useful from a data science competition standpoint, they have limited clinical utility because of their narrow focus on one single diagnostic task. For example, the two Kaggle CXR competitions hosted by RSNA and SIIM have focused on diagnosis of a single disease – pneumonia and pneumothorax (Yi et al., 2021). Although impressive results have resulted from these competitions, their utility is limited given the dozens of diagnoses that could present in real-world clinical practice and the possibility of a patient being diagnosed with both pneumonia and pneumothorax. Since both datasets are subsets of the larger NIH dataset – out of the 2495 patients diagnosed with either pneumonia or pneumothorax, 185 patients were diagnosed with both, as shown in Appendix Figure 3. Thus, making both toy datasets, and any other derivatives of the NIH dataset, incomplete.

Therefore, a method to harmonize these large-scale as well as toy datasets to train a clinically-useful model could revolutionize how distributed and incomplete datasets with different disease labels can be leveraged in aggregate for development of clinically-relevant deep learning models. To that end, we propose surgical aggregation, a federated learning (FL) framework for aggregating knowledge from spatially distributed datasets with incomplete and different disease annotations into a ‘global’ meta-deep learning model. In this work, we demonstrate the potential for surgical aggregation to develop clinically useful deep learning models by aggregating knowledge from distributed datasets with diverse tasks.

2. Prior Research

Federated learning (FL) is a collaborative machine learning technique that approaches the problem of training a ‘global’ model on non-iid data from a multi-domain and multi-task perspective. By using a decentralized and distributed approach, consisting of a central server and nodes, a global model can be trained to generalize distributed tasks with non-iid labels. In the realm of medical imaging, FL has enabled training of large-scale ‘global’ deep learning models using homogenous data spread across multiple institutions without sharing sensitive patient data (Rieke et al., 2020; Chowdhury et al., 2022). However, majority of the datasets being curated across the world are heterogenous and focus on similar but different tasks. Consequently, different strategies and heuristics have been proposed in the literature for aggregating knowledge from heterogeneous datasets (Gong et al., 2021, 2022; Kulkarni et al., 2022; Arasteh et al., 2022).

Knowledge distillation has emerged as a popular technique across multiple domains for aggregating knowledge from heterogeneous datasets (Li and Wang, 2019; Chang et al., 2019; Gong et al., 2021, 2022; Kulkarni et al., 2022). Gong et al. (2022) explored an ensemble attention distillation based FL approach to harmonize the NIH and CheXpert datasets, demonstrating the ability to train a global model with 14 disease labels, with 12 from CheXpert and 8 from the NIH dataset. However, the proposed approach required a separate external dataset and worked only in a multi-class scenario i.e. a patient could not be diagnosed with more than one disease, making it practically challenging. Alternatively, a different approach, proposed recently, involved aggregating only the network backbone during FL training (Arasteh et al., 2022). However, this approach involved further training of the local models post FL aggregation resulting in different local models optimized for their respective tasks as opposed to a single multi-task global model.

In this work, we propose surgical aggregation wherein the server surgically aggregates relevant knowledge coming in from each node to effectively learn different tasks across all the datasets. Our proposed technique does not require any additional external dataset for training and is developed to handle scenarios where contributing datasets contain different, overlapping, and incomplete labels. We evaluated surgical aggregation on synthetic toy datasets created from the NIH Chest X-Ray 14 dataset as well as on aggregating knowledge from NIH Chest X-Ray 14 and CheXpert datasets into a ‘global’ model.

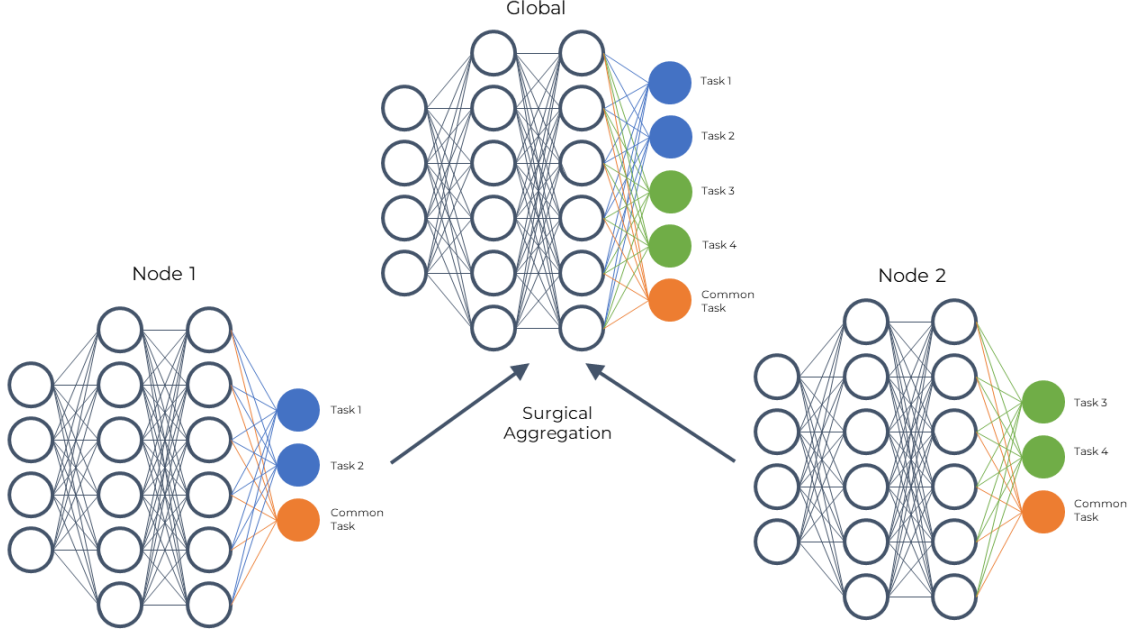


Figure 2: An overview of the surgical aggregation framework.

3. Methods

3.1. Surgical Aggregation

We developed surgical aggregation as a model and task-agnostic framework for ‘surgically’, i.e. selectively, aggregating weights corresponding to a certain diagnostic task during the aggregation step of each FL round. Let’s consider K datasets with L_1, L_2, \dots, L_K diseases labels, with or without overlapping labels. By utilizing surgical aggregation, the global model can predict the presence of all $\bigcup_{i=1}^K L_i$ unique disease labels present across all K datasets, as visualized in Figure 2.

We initialized our FL setup as a multi-task and multi-label deep neural network composed of a central server and two nodes. The model consists of two distinct blocks - a representation block and a task block. In such a setup, the representation block learns a generalized global representation of the data using extracted feature semantics while the task block learns to interpret this representation and predict the presence of abnormalities. During training, the weights corresponding to the representation block are always aggregated and redistributed by the central server back to the nodes, thereby developing a generalized representation for different tasks in the representation block. In contrast, The weights from each task block are surgically aggregated to aggregate task-related knowledge from each node into a global task block. If a disease label is shared across one or more nodes, the weight and bias applied to the input of the neuron corresponding to that label in the task block are aggregated using a predefined strategy (for eg., FedAvg). However, if a disease label is unique to the node, the weights remain unchanged. This enables the selective aggregation of the weights applied to the input of the task block and enables the

global model to construct a task block that is an aggregation of the knowledge learned for all disease labels from all nodes. The surgical aggregation framework is described in detail in Algorithm 1.

In our implementation, we utilized a **DenseNet121** model architecture, initialized with ImageNet weights. For weight aggregation for both representation and task blocks, we implemented Federated Averaging **FedAvg**, as described in [McMahan and more \(2017\)](#). The surgical aggregation was applied to the final fully-connected Dense classification layer.

Algorithm 1: Surgical Aggregation

Input: K clients indexed by k , with local labels L_k and final Dense layer weights w_k ;
 Predefined weight aggregation strategy **aggregate**;

Output: w_g , the final Dense layer weights for the global model

$$L_g \leftarrow \bigcup_{k=1}^K L_i$$

```

for  $i \leftarrow 1$  to  $\text{len}(L_g)$  do
   $w_{agg} \leftarrow []$ 
  for  $k \leftarrow 1$  to  $K$  do
    if  $L_g[i]$  in  $L_k$  then
      | append  $w_k$  to  $w_{agg}$ 
    end
  end
   $w_g[i] \leftarrow \text{aggregate}(w_{agg})$ 
end

```

3.2. Datasets

3.2.1. NIH CHEST X-RAY 14

The NIH dataset, curated by [Wang et al. \(2017\)](#), consists of 14 disease labels (Figure 1) with 112,120 frontal-view CXRs from 30,805 unique patients. We randomly divided the dataset into training (70%), validation (10%), and testing (20%) splits while ensuring no patient appears more than once in each split.

We further divided the training and validation splits for conducting two experiments. For the first experiment, we randomly pruned the disease labels to create two distributed and incomplete toy datasets containing 11 and 8 labels respectively with 4 overlapping labels, as described in Appendix Figure 4(a). Similarly, for the second experiment, we randomly pruned the disease labels to create two disjoint distributed and incomplete toy datasets with 7 labels each, as described in Appendix Figure 4(b).

3.2.2. CHEXPERT

The Stanford CheXpert dataset, curated by [Irvin et al. \(2019\)](#), consists of 13 disease labels (Figure 1) and an additional label for ‘normal’ with 224,316 CXRs from 65,240 unique patients. To handle uncertain labels in the dataset, we chose the U-Ones approach i.e. treating all uncertain labels as positive. We randomly divided the dataset into training (70%), validation (10%), and testing (20%) splits while ensuring no patient appears more than once in each split.

3.3. Experimental Setup

We conducted two preliminary experiments to evaluate the surgical aggregation framework for toy datasets, with overlapping and disjoint disease labels respectively, sampled from the NIH dataset, as described in Section 3.2.1. The surgically aggregated global model for both experiments would result in a model that can predict all 14 disease labels present in the NIH dataset. We compared the performance of both global models to a baseline model trained on complete training and validation data using the held-out internal testing set. Additionally, we trained a model for both experiments without utilizing surgical aggregation and naïvely concatenated both incomplete toy datasets. This would allow us to establish an upper and lower bound for the expected performance of the surgically aggregated global models. For further validation of our methods, we utilized the surgical aggregation framework to train a generalized global model that harmonizes the NIH and CheXpert datasets. Our surgically aggregated global model would result in a model that can predict all 20 unique disease labels present across both datasets, with 7 overlapping labels. We compared the performance of the resultant global model using held-out internal testing sets from both datasets to baseline models trained individually on both.

We computed the area under receiver operating characteristic (AUROC) curve for each model. The average and disease label-wise AUROC score between the global model and baseline models were compared using bootstrapping and paired t-test. For all experiments, statistical significance was defined as $p < 0.05$.

4. Results

When evaluating the performance of the surgically aggregated global model on two toy datasets with overlapping disease labels, we observed excellent overall performance in diagnosing all 14 disease labels in a held-out testing set from the NIH dataset. We observed comparable performance with the baseline model trained on complete data when comparing the AUROC scores across every disease label. Furthermore, we demonstrated that utilizing surgical aggregation to harmonize toy datasets resulted in a significant improvement in model performance when compared to naïvely concatenating the datasets to train a model with incomplete information. The results of the following are detailed in Table 1 and 2.

Model	Loss	AUROC
Baseline	0.15	0.87
Näive	0.16	0.85 (<0.001)
Surgical Aggregation	0.15	0.87 (0.54)

Table 1: Average model metrics for toy datasets with overlapping disease labels from the NIH dataset. p-value provided in brackets.

Similarly, when evaluating the performance of the surgically aggregated global model on two toy datasets with disjoint i.e. no overlap between disease labels, we observed excellent overall performance in diagnosing all 14 disease labels in the held-out testing set from the NIH dataset. Unfortunately, in this experiment, we observed a statistically significant

Disease Label	Baseline	Näive	Surgical Aggregation
Atelectasis	0.79	0.77 (<0.001)	0.78 (0.01)
Cardiomegaly	0.89	0.89 (0.87)	0.89 (0.95)
Consolidation	0.81	0.80 (0.09)	0.81 (0.74)
Edema	0.89	0.87 (<0.001)	0.89 (0.48)
Effusion	0.87	0.87 (0.95)	0.87 (0.51)
Emphysema	0.89	0.89 (0.85)	0.89 (0.78)
Fibrosis	0.75	0.73 (0.10)	0.75 (0.80)
Hernia	0.84	0.86 (0.64)	0.83 (0.74)
Infiltration	0.69	0.68 (0.02)	0.69 (0.94)
Mass	0.85	0.85 (0.71)	0.85 (0.56)
Nodule	0.74	0.72 (0.01)	0.73 (0.07)
Pleural_Thickening	0.78	0.75 (<0.001)	0.76 (0.08)
Pneumonia	0.73	0.72 (0.41)	0.72 (0.74)
Pneumothorax	0.87	0.85 (0.01)	0.86 (0.19)

Table 2: Disease label-wise model’s AUROC scores for toy datasets with overlapping disease labels from the NIH dataset. p-value provided in brackets.

drop in performance when compared to the baseline model on average and across every disease label. Despite this shortcoming, we have yet again demonstrated that utility of surgical aggregation to harmonize toy datasets with an improvement in model performance when compared to naïvely concatenating the datasets to train a model with incomplete information. The results of the following are detailed in Table 3 and 4.

Model	Loss	AUROC
Baseline	0.15	0.87
Näive	0.17	0.84 (<0.001)
Surgical Aggregation	0.15	0.86 (<0.001)

Table 3: Average model metrics for toy datasets with disjoint disease labels from the NIH dataset. p-value provided in brackets.

Finally, when evaluating the performance of utilizing surgical aggregation to harmonize the NIH and CheXpert datasets, we observed a significant drop in performance when compared to baseline models trained individually on both datasets. However, despite performing poorer, we have demonstrated the ability of surgical aggregation in harmonizing and aggregating knowledge from two distributed and incomplete large-scale datasets to detect the presence of 20 unique abnormalities (Figure 1) in the thorax. The results are detailed in Table 5.

Disease Label	Baseline	Näive	Surgical Aggregation
Atelectasis	0.79	0.76 (<0.001)	0.77 (<0.001)
Cardiomegaly	0.89	0.84 (<0.001)	0.85 (<0.001)
Consolidation	0.81	0.80 (0.02)	0.79 (0.03)
Edema	0.89	0.87 (0.01)	0.88 (0.06)
Effusion	0.87	0.85 (<0.001)	0.85 (<0.001)
Emphysema	0.89	0.85 (<0.001)	0.87 (0.01)
Fibrosis	0.75	0.74 (0.36)	0.75 (0.99)
Hernia	0.84	0.87 (0.52)	0.86 (0.76)
Infiltration	0.69	0.68 (0.01)	0.69 (0.28)
Mass	0.85	0.80 (<0.001)	0.81 (<0.001)
Nodule	0.74	0.72 (0.01)	0.71 (<0.001)
Pleural_Thickening	0.78	0.75 (<0.001)	0.76 (0.08)
Pneumonia	0.73	0.71 (0.21)	0.74 (0.64)
Pneumothorax	0.87	0.84 (<0.001)	0.85 (<0.001)

Table 4: Disease label-wise model’s AUROC scores for toy datasets with disjoint disease labels from the NIH dataset. p-value provided in brackets.

Model	NIH		CheXpert	
	Loss	AUROC	Loss	AUROC
NIH Baseline	0.15	0.87	-	-
CheXpert Baseline	-	-	0.39	0.84
Surgical Aggregation	0.16	0.85 (<0.001)	0.44	0.83 (<0.001)

Table 5: Average model metrics for surgically aggregated global model that harmonizes the NIH and CheXpert datasets.

5. Discussion

Although the release of public and curated large-scale CXR datasets has spearheaded the utility of deep learning models in detecting the presence of common, and often life-threatening, diseases using CXRs, training a large-scale model that aggregates knowledge from these distributed and incomplete datasets has held back the clinical utility of such models. Despite our methods resulting in models performing worse than models trained on complete data, our results demonstrate that surgical aggregation could potentially be used to develop clinically useful deep learning models by aggregating knowledge from distributed datasets with diverse tasks and open new avenues for the development of newer FL aggregation strategies as well as further research into the field of harmonizing distributed and incomplete large-scale datasets in hopes of surgically aggregating crucial knowledge from each dataset to train a clinically-useful large-scale global model – a step forward towards bridging the gap from bench to bedside.

References

Soroosh Tayebi Arasteh, Peter Isfort, Marwin Saehn, Gustav Mueller-Franzes, Firas Khader, Jakob Nikolas Kather, Christiane Kuhl, Sven Nebelung, and Daniel Truhn. Collaborative training of medical artificial intelligence models with non-uniform labels. *arXiv preprint arXiv:2211.13606*, 2022.

Hongyan Chang, Virat Shejwalkar, Reza Shokri, and Amir Houmansadr. Cronus: Robust and heterogeneous collaborative learning with black-box knowledge transfer. *arXiv preprint arXiv:1912.11279*, 2019.

Alexander Chowdhury, Hasan Kassem, Nicolas Padoy, Renato Umeton, and Alexandros Karargyris. A review of medical federated learning: Applications in oncology and cancer research. In *International MICCAI Brainlesion Workshop*, pages 3–24. Springer, 2022.

Xuan Gong, Abhishek Sharma, Srikrishna Karanam, Ziyan Wu, Terrence Chen, David Doermann, and Arun Innanje. Ensemble attention distillation for privacy-preserving federated learning. In *Proceedings of the IEEE/CVF International Conference on Computer Vision*, pages 15076–15086, 2021.

Xuan Gong, Liangchen Song, Rishi Vedula, Abhishek Sharma, Meng Zheng, Benjamin Planche, Arun Innanje, Terrence Chen, Junsong Yuan, David Doermann, et al. Federated learning with privacy-preserving ensemble attention distillation. *IEEE Transactions on Medical Imaging*, 2022.

Jeremy Irvin, Pranav Rajpurkar, Michael Ko, Yifan Yu, Silviana Ciurea-Ilcus, Chris Chute, Henrik Marklund, Behzad Haghgoo, Robyn Ball, Katie Shpanskaya, et al. CheXpert: A large chest radiograph dataset with uncertainty labels and expert comparison. In *Proceedings of the AAAI conference on artificial intelligence*, volume 33, pages 590–597, 2019.

Alistair EW Johnson, Tom J Pollard, Nathaniel R Greenbaum, Matthew P Lungren, Chih-ying Deng, Yifan Peng, Zhiyong Lu, Roger G Mark, Seth J Berkowitz, and Steven Horng. Mimic-cxr-jpg, a large publicly available database of labeled chest radiographs. *arXiv preprint arXiv:1901.07042*, 2019.

Pranav Kulkarni, Adway Kanhere, Paul H Yi, and Vishwa S Parekh. From competition to collaboration: Making toy datasets on kaggle clinically useful for chest x-ray diagnosis using federated learning. *arXiv preprint arXiv:2211.06212*, 2022.

Daliang Li and Junpu Wang. Fedmd: Heterogenous federated learning via model distillation. *arXiv preprint arXiv:1910.03581*, 2019.

Brendan McMahan and more. Communication-Efficient Learning of Deep Networks from Decentralized Data. In *Proceedings of the 20th International Conference on Artificial Intelligence and Statistics*, volume 54 of *Proceedings of Machine Learning Research*, pages 1273–1282. PMLR, 20–22 Apr 2017.

Ha Q Nguyen, Khanh Lam, Linh T Le, Hieu H Pham, Dat Q Tran, Dung B Nguyen, Dung D Le, Chi M Pham, Hang TT Tong, Diep H Dinh, et al. Vindr-cxr: An open dataset of chest x-rays with radiologist’s annotations. *Scientific Data*, 9(1):1–7, 2022.

Nicola Rieke, Jonny Hancox, Wenqi Li, Fausto Milletari, Holger R Roth, Shadi Albarqouni, Spyridon Bakas, Mathieu N Galtier, Bennett A Landman, Klaus Maier-Hein, et al. The future of digital health with federated learning. *NPJ digital medicine*, 3(1):1–7, 2020.

George Shih, Carol C Wu, Safwan S Halabi, Marc D Kohli, Luciano M Prevedello, Tessa S Cook, Arjun Sharma, Judith K Amorosa, Veronica Arteaga, Maya Galperin-Aizenberg, et al. Augmenting the national institutes of health chest radiograph dataset with expert annotations of possible pneumonia. *Radiology. Artificial intelligence*, 1(1), 2019.

Xiaosong Wang, Yifan Peng, Le Lu, Zhiyong Lu, Mohammadhadi Bagheri, and Ronald M Summers. Chestx-ray8: Hospital-scale chest x-ray database and benchmarks on weakly-supervised classification and localization of common thorax diseases. In *Proceedings of the IEEE conference on computer vision and pattern recognition*, pages 2097–2106, 2017.

Paul H Yi, Tae K Kim, E Siegel, and Yahyavi-Firouz-Abadi N. Demographic reporting in publicly available chest radiograph data sets: Opportunities for mitigating sex and racial disparities in deep learning models. *Journal of the American College of Radiology*, 19(1 Pt B):192–200, 2021.

Appendix A. Disease Label Overlap in Diagnosed Patients

The co-occurrence matrix of disease labels, visualized in Appendix Figure 3, for all diagnosed patients from the NIH dataset demonstrates the overlap of every disease label in the dataset with another label for every patient who is diagnosed. As a result, any derivative of the NIH dataset focusing on a single diagnostic task is inherently incomplete. The co-occurrence matrix was calculated by first determining the positive disease labels for each patient across all available studies and then determining the number of patients that have been diagnosed for each disease label.

Appendix B. Disease Label Distribution for Synthetic Toy Datasets

The disease label distribution for synthetic toy datasets created for utilizing surgical aggregation to harmonize datasets with overlapping and disjoint labels is described in Appendix Figures 4(a) and 4(b).

SURGICAL AGGREGATION

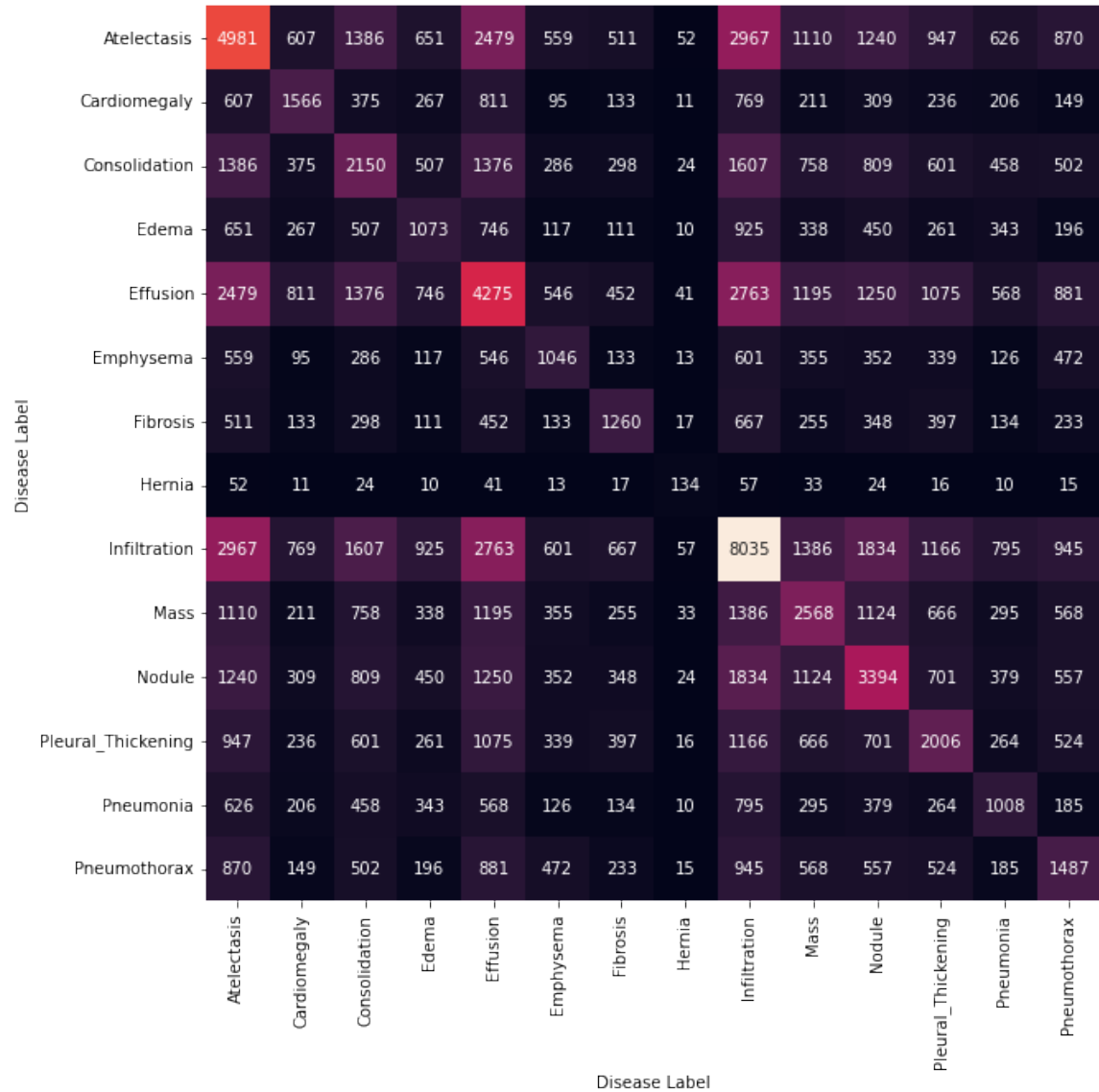


Figure 3: Co-occurrence matrix of disease labels for diagnosed patients from the NIH dataset.

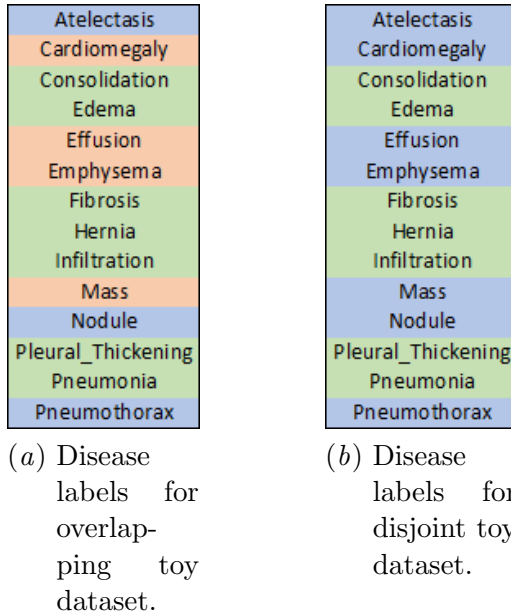


Figure 4: Distribution of disease labels from NIH dataset across both nodes for surgical aggregation experiment. All labels in first node highlighted in green, second node highlighted in blue, and all overlapping labels highlighted in orange.